applied optics

Combined method for the fabrication of high-power cladding light stripper using a buffered oxide etchant

Elif Yapar Yildirim, Ali Karatutlu, Ekin Teslime Balk, Yakup Midilli, and Bülend Ortaç*

UNAM-National Nanotechnology Research Center and Institute of Material Science and Nanotechnology, Bilkent University, 06800 Ankara, Turkey
*Corresponding author: ortac@unam.bilkent.edu.tr

Received 8 March 2019; revised 11 July 2019; accepted 26 July 2019; posted 30 July 2019 (Doc. ID 361916); published 29 August 2019

Cladding light strippers (CLSs) are vital and one of the critical components for high-power fiber laser applications. In this study, we show the first studies of the formation mechanisms and optimum conditions of a CLS device using a buffered oxide etchant by a combined method of stain (wet) etching and vapor-phase etching. This high-power CLS was shown to result in a stripping performance of ~17.2 dB at the launched power of 333 W (pump limited). The thermal imaging demonstrates that the maximum temperature reached when operating the device at maximum launched power was ~75°C. The atomic force microscopy (AFM) results show that the combined method yields crystal-like structures with the height in microscales, whereas other conventional methods give only nanoscale roughness. The method also preserves the diameter of the CLS device close to the bare fiber with about 10 μm tapering leads to a high surface area to strip unwanted light, which is good for heat dissipation. The combined method possesses the outcome of two methods, including both the crystal-like structures and nanosized hillocks, resulting in high-power stripping performance and robustness.

https://doi.org/10.1364/AO.58.006926

1. INTRODUCTION

The cladding light in the fiber laser and amplifiers become important particularly in high-power applications. This cladding light includes the residual (unabsorbed) pump light, amplified spontaneous emission of the active core fiber, cladding mode signal light due to the difference in the refractive indices (RIs) of inner and outer claddings, light leaking due to imperfect splices, and bend losses causing backward signal radiation. Therefore, removing such cladding light is a prerequisite for the quest of obtaining a single-mode fiber laser and its long-term operation at high power. In kilowatt-level applications, the cladding light stripper (CLS) should be designed for the operation on the order of 100 W.

Various approaches were utilized in the formation of the high-power CLS. These are (i) hydrofluoric acid (HF) etching with acidic fluorides [1,2], (ii) cascaded coating of the fibers using UV-curable polymers with various RIs [3,4], (iii) soft metal coating, (iv) surface texturization using lasers [5,6], and (v) high-index capillary coating [7,8].

All these methods have their advantages and disadvantages as follows: (i) Working with HF and acidic fluorides requires a great deal of attention, but this method appears to be successful at attenuating 27 dB of the pumped light with the NA of 0.44 [1]. Furthermore, the etched fiber can be tapered despite the fact that the term "tapering" is generally used upon applying the heat-pull method but can also be referred to for acidic tapering [9]. In acidic tapering, only the cladding is tapered; thus, the signal light is not perturbed as compared to the heat-pull method. However, there seem to be an issue in the removal of light with low NA, and the fiber can become, respectively, more fragile after etching. (ii) Cascaded coating with the UV-curable polymers were shown to be promising due to an opportunity to remove the cladding lights with different NAs. However, polymer degradation over the operation time and local heating can be an issue, particularly due to the large thickness of the coatings (on the order of 15 μm). On the other hand, there is almost no information about the polymers used in the CLS, such as their names and preparation, etc., unlike their RIs. (iii) The soft metal coating is another promising approach, but current studies show the CLS performance is highly dependent on the metal used. For example, Sn and Au coatings can cause local heating during stripping most of the unwanted cladding light. On the other hand, the stripping capability of the CLS needs to be developed using In and Al. (iv) The surface texturization method using a laser source produce micromachining [5] or deposition [6] of different geometries on the fiber glass surface. The texture behaves similar to the CLS prepared by etching in principle. (v) Capillary coating includes mostly collapsing a thicker fiber on the top of a thinner one, as the latter includes the active core. The collapsed fiber

has a higher RI with respect to the cladding of the active core. Nevertheless, this method also requires a surface texturization process using HF etching or a CO_2 laser [7]. Or it may require a high-index thermal paste [8], which causes stability issues in the long term and does not stand up to the high powers. As a result, a simpler, safer, and relatively more effective method for the preparation of the CLS is highly demanded. And this should be applicable in the large scale for high-power laser applications.

Many groups have demonstrated CLSs fabricated by coating and/or etching methods. These include [5] the high-index polymer with 18 dB loss [4], the soft metal coating with 20 dB loss [10], an interesting study on high-power CLS preparation with 20 dB using recoating fiber surface with a capillary glass [8], and chemical etching methods with 27 dB and 16.7 dB loss [1,7,9]. However, no detailed studies on the precise information about the optimum etching conditions and utilizing different chemical etching methods, including chemical stain etching and vapor-phase etching were reported on the performance of CLSs.

In this paper, an improved cladding light stripping method is presented via a benchtop chemical etching method. In particular, we focused on clarifying the effects of the different morphological structures obtained using the above-mentioned chemical etching methods on obtaining the better performance of a CLS device and report the effect of fluoride etching on the morphology of silica surfaces in addition to the CLS performance. In other words, we report the physical formation mechanisms of the structures together with the reproducibility of the results. When combining this information with specific performance knowledge, it can be used to choose the required process during the CLS fabrication. In this context, fibers were prepared, fluoride etching of fibers was performed, and after characterizing the surface morphology, the device performances were tested. And, an all-glass device provides a cladding stripping loss of ∼17.2 dB in a 400 μm diameter and 12 cm length. The total power of 333 W from two diodes is launched into the cladding of the fiber at the input to the cladding stripper, and 6.2 W of remaining radiation is measured at the output. The thermal images of the packaged device are presented.

2. MATERIALS AND METHODS

A. Materials

For the device fabrication, all passive fibers were purchased from nLIGHT (Liekk Passive-20/400DC). Buffered oxide etchant (BOE) 7:1 ($HF:NH_4F = 12.5:87.5\%$) was supplied in very large scale integration quality and the polytetrafluoroethylene baths were designed and produced in-house in different dimensions and are shown in Fig. 1(a). All chemicals were used as purchased from Sigma-Aldrich.

B. Device Fabrication

Passive fibers (20/400) were window-stripped by using a coating stripper (Model: Fujikura PCS-100). Then, the fibers were cleaned by isopropyl alcohol (IPA) and deionized (DI) water before being placed in the PTFE bath. After these preparation steps, we fabricate three different CLS devices to be tested by using the stain etching method first (Device A), second, the vapor-phase etching method (Device B), and the combined method of stain etching and vapor-phase etching method (Device C). The experimental conditions such as ambient temperature/pressure/humidity were kept constant. All chemical etching processes using BOE solution were conducted using the PTFE bath in a cleanroom environment at room temperature. The typical image of the fabricated CLS is given in Fig. 1(b).

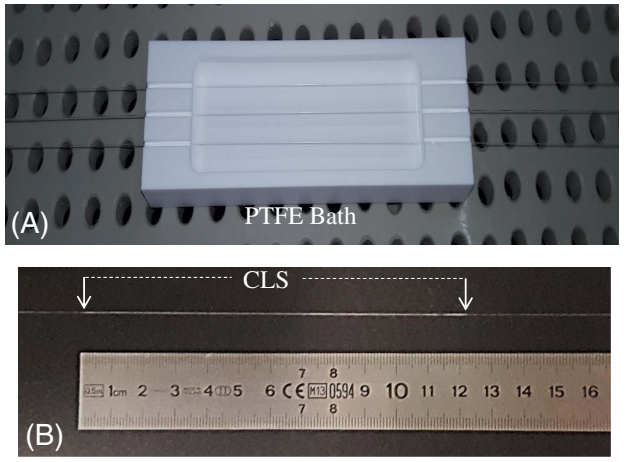

Fig. 1. (A) PTFE bath used for the mass scale device fabrication designed for 12 cm length of the CLS; (B) fabricated 12 cm length of CLS.

Device A: The chemical stain etching method using the BOE solution was applied to the window-stripped fiber having a length of 12 cm for an optimum of 16.5 h. After the formation of the device in the BOE solution, the fiber was washed thoroughly with the DI water and then dried by a flow of nitrogen gas.

Device B: The window-stripped fiber was placed onto the channel of the PTFE bath without any contact with the BOE solution and only exposed to the BOE vapor for 16.5 h. Then, the fiber was washed with the DI water and then was dried by the flow of a nitrogen gas.

Device C: The stripped fiber at the length of 12 cm was immersed inside the BOE in the PTFE bath for 5 s. Such short duration was chosen in order to prevent the extensive tapering of the stripped fiber. This process could be considered to be an immediate process of the stain-etching method mentioned for Device A. Then, without any cleaning procedure, the fiber was kept just above the BOE solution and then the BOE vapor was exposed onto the sample surface. Next, the cover of the PTFE bath was closed, and the process was ended at the end of 16.5 h. The vapor-phase etching procedure was applied for different durations from 1 h to 72 h, and 16.5 h was found to be sufficient and optimum for obtaining the preparation conditions of Device C. The cleaning procedure was repeated after the etching process was completed. The differences in the fabrication methods of the devices are briefly represented in Table 1.

C. Device Characterization and Performance Tests

The morphology and structure of the samples were investigated by using scanning electron microscopy (SEM, Model: FEI

Table 1. Differences in the Fabrication of the Devices

Device	Etchant	Time	Length (cm)	Method
A	BOE solution	16.5 h	12	Stain etching
B	BOE vapor	16.5 h	12	Vapor-phase etching
C	BOE solution	5 s	12	Combined method
	BOE vapor	16.5 h		

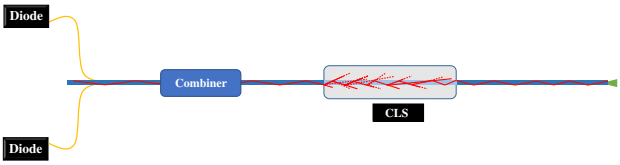

Fig. 2. Schematic presentation of the device characterization setup.

NanoSem) technique and scanning probe microscope (SPM) technique (AFM PSIA XE-100). In the SPM measurements, an AFM tip made of silica coated by aluminum with a diameter of 10 nm was utilized in contact mode. XEI software was operated for the data collection and analyses. The energy-dispersive x-ray spectroscopy (EDS) measurements were collected by using the SEM technique at 10 kV voltages. The structural properties of the devices were investigated using Raman spectroscopy (Model: Witec SNOM Raman 300 Alpha coupled with a diode laser at $\lambda = 532$ nm).

The power-handling capability of the devices was tested with an experimental setup (Fig. 2), which includes two pumping diodes (Model: Dilas, at $\lambda = 976$ nm, maximum power = 333 W), a DC power supply, pump combiners, homemade aluminum water cooling block, and a power meter (Model: Ophir 30A-P-17, operating range, 60 mW–30 W) on an optical table. All tests were performed while the heat-sinking system was set to keep the temperature of the circulating water constant at 20°C. This was performed via two chillers (Model: OMI CHWM21 and Model: Neslab Merlin M25), and we focused especially on the homemade aluminum water cooling block that holds the fiber in and thermally disconnects the fiber from the heat generated by the scattered light along the CLS. During the device performance tests, the radiation propagates through the cladding of fiber. This process was observed by a near-infrared (NIR) viewer (Model: EMO Electronic GmbH). Furthermore, a thermal camera (Model: FLIR Thermo-vision A40) was operated to control the temperature and the stability of the characterization setup and the device.

3. RESULTS AND DISCUSSION

First, the morphological features of the CLS devices, including Devices A, B, and C were investigated using the SEM technique (Fig. 3). The insets show the respective structural differences of the devices. For Device A, obtained only using the stain-etching method, we observed that the fiber has extensively tapered from 400 μm to 260.6 μm in diameter. In the inset of Fig. 3(a), crystal-like shapes [1] on the order of 40–50 μm were clearly observed on the surface of Device A. Operation of the vapor-phase etching method created by Device B with a diameter of 392.6 μm was observed to be

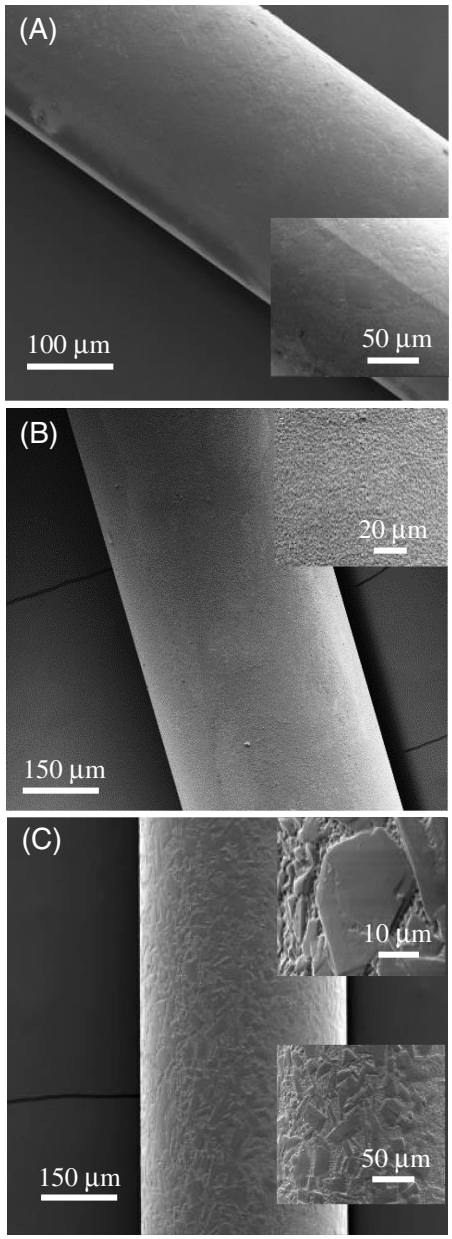

Fig. 3. SEM images of etched fiber cladding fabricated by different methods. (A) Chemical stain etching; (B) vapor-phase etching; (C) combined method of (A) and (B).

barely changed compared to the initial fiber diameter. In the inset of Fig. 3(b), only relatively much smaller hillocks with a mean size of 2.9 ± 1.9 μm out of 413 hillocks were observed to be formed on Device B. In the combined method, where the stain-etching method and the vapor-phase etching method were used, Device C was fabricated with a diameter of 390.6 μm. This emphasizes that the combined method did not taper the fiber excessively, as was the case in which only the stain-etching method was employed. In the insets of Fig. 3(c), mainly two types of the morphological structures are shown, as expected. These two structures, consisting of (i) the crystal-like shapes and (ii) the hillocks, are the outcome of the first two methods, including the stain-etching method and the

vapor-phase etching method, respectively. These results demonstrate that the structural motifs were preserved in the combined method by a slight change in the diameter.

Figure 4 demonstrates SEM images of three different batches (C-1, C-2, C-3) for Device C. Similar topologies are observed to be obtained upon applying the combined method, although there could be some minor deviations in the experimental conditions, such as duration of etching both in the instantaneous (~5 s) stain etching and the vapor-phase etching, the ambient temperature, and distance between the surface of the bare fiber and BOE solution in the vapor-phase etching process. We would like to point out that these minor deviations were not prevented and do not affect formation of the crystal-like structures and the nanosized hillocks on the fiber surface.

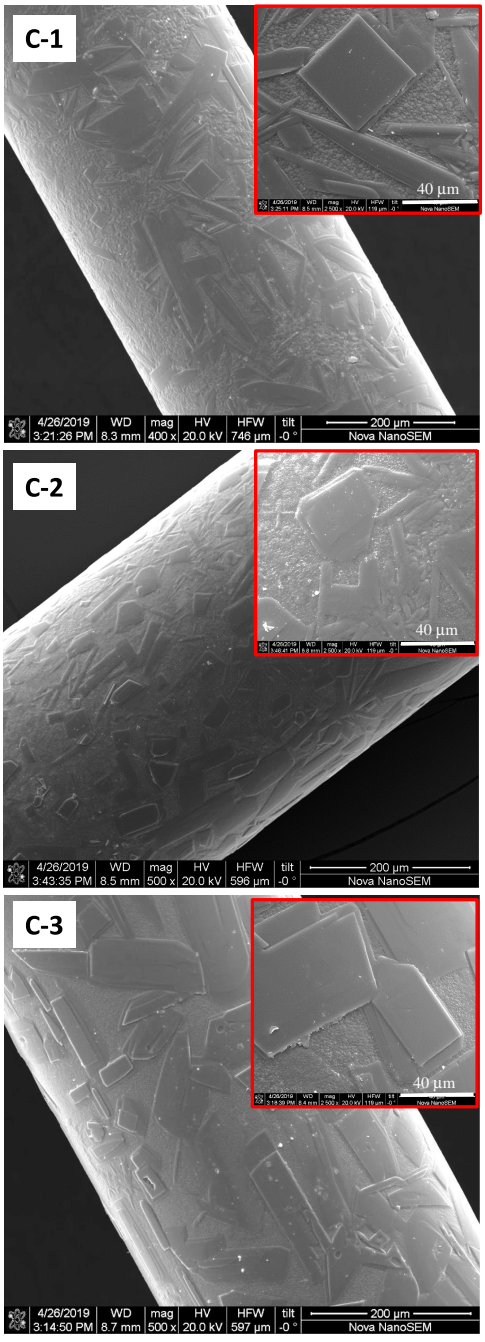

Fig. 4. SEM images of the devices (Device C) fabricated by the combined method, representing repeatability of the method.

The SEM results are shown in Fig. 3. A and C imply the differences in the height of crystal-like shapes between Devices A and C. However, for the quantitative analyses, we performed the AFM studies [Figs. 5(a)–5(c)], which were used to explore the surface topology further and to determine the height of the shapes. The AFM results show that Device A [Fig. 5(a)] has the crystal-like shapes with a height of ~400 nm, and Device B [Fig. 5(b)] has rather ordered shapes from 250 to 260 nm height in nanoscale and a roughness (Ra) of 16.1 nm. Henceforth, we use the term "nanosized hillocks" for these structures, which is consistent with previous studies [11] where the same description was used. The combined method [Device C, Fig. 5(c)] has generated the crystal-like shapes as observed in the case of the stain-etching method (Device A) but also given an opportunity to obtain these structures to be in micrometer-scale both in width and height, which are

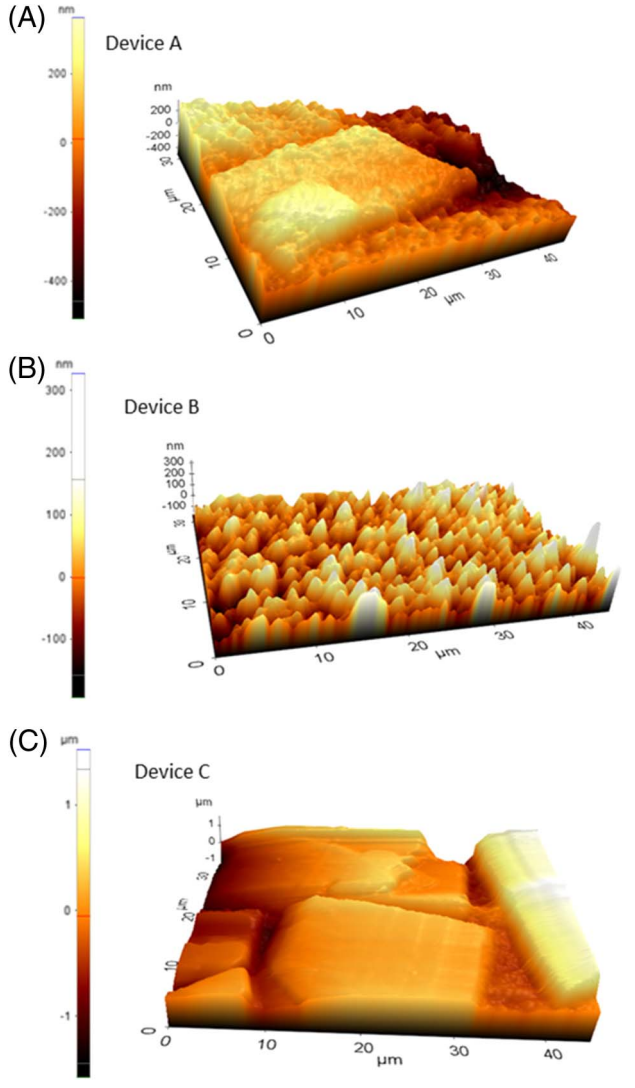

Fig. 5. AFM images of the CLS devices fabricated by different methods. (A) Chemical stain-etching method; (B) vapor-phase etching method; (C) combined method.

considered to be required to scatter most of the unwanted light in micrometer wavelength [1,3].

In the formation process of Devices A, B, and C, the etching methods are applied to the stripped fibers to get the light-scattering structures, in which both height and width are important, to obtain high performance from the device, as mentioned above. These structures are formed by the etching of silicate cladding surface by the HF in the presence of ammonium fluoride (NH_4F). So, to etch the silicate glasses, we use BOE as a reagent to form the bifluoride ions *in situ* by producing fluoride (F^-) and hydrogen (H^+) ions. NH_4F is used as a F^- ions source [Eq. (2)] and so for the formation of HF_2^- ions from undissociated HF [Eq. (3)].

If we use HF as an etching solution, HF leads to dissolution of silicate glasses [2,12,13],

$$SiO_2 + 6HF \rightarrow SiF_6^{2-} + 2H_2O + 2H^+. \quad (1)$$

In the case of BOE, silica is dissolved by the reaction [11],

$$SiO_2 + 4HF \rightarrow SiF_4 + 2H_2O. \quad (2)$$

Then the product of this reaction (SiF_4) diffuses from the glass and forms precipitation with the salt, diffusing in the opposite direction from the solution to the fiber surface [11],

$$SiF_4 + 2HF + 2NH_4^+ \rightarrow (NH_4)_2SiF_6 + 2H^+. \quad (3)$$

The formation of stable hexafluoride silicate anion [14] involves many steps and intermediates like formation of H^+ and F^- anions [15],

$$HF \rightarrow H^+ + F^-. \quad (4)$$

This F^- ion reacts to form the bifluoride anion (HF_2^-),

$$HF + F^- \rightarrow HF_2^-. \quad (5)$$

This HF_2^- is the primary species for the attacking of silica matrix [14] by replacing the divalent oxygen anions from silicon-oxygen tetrahedron $(SiO_4)_4^-$ and destroying the glass network. In Devices A and C, these crystal-like structures start to form immediately when we insert the fiber into the BOE solution and go on from the solution and exposure to BOE vapor (Device C) or leave the fiber in the BOE solution (Device A). As a result, after a very rapid formation of hexafluorosilicates (silicofluoride crystals) [Eq. (3)] [1,15,16], these silicofluorides were observed in contact with the fiber surface immediately and prevent etching of this area. The Raman results (Fig. 6) show intense and broad Raman bands at 433 cm^{-1} and 484 cm^{-1}. The bands within this region are generally assigned to A1:deformation mode or bond-rocking motions [17]. On the other hand, Raman modes observed at 484 cm^{-1} and 598 cm^{-1} can also be attributed to the defect centers in the fused silica [18]. The symmetric stretching mode at 795 cm^{-1} and antisymmetric stretching mode at 1057 cm^{-1} and 1194 cm^{-1} were observed for O-Si-O bonds.

The fluorine content in silica above 5% F doping appears to result in a new peak at about 945 cm^{-1} [19]. However, this mode was not observed in the Raman data of all the samples. F-doped silica can also lead to the O-Si-O linkages split observed near 1170 cm^{-1}. The latter was observed for Devices A and B and are represented within Figs. 6(a) and 6(b), respectively. From these results, it could be inferred that the fluorine content could be less than 5% upon the treatment of the BOE solution. The fingerprint region of NH_4F takes place in about 3000 cm^{-1}, including main $\nu(A1 + E1 + E2)$ and $\nu(A1)$ modes at 2818 cm^{-1} and 2876 cm^{-1}, respectively [20].

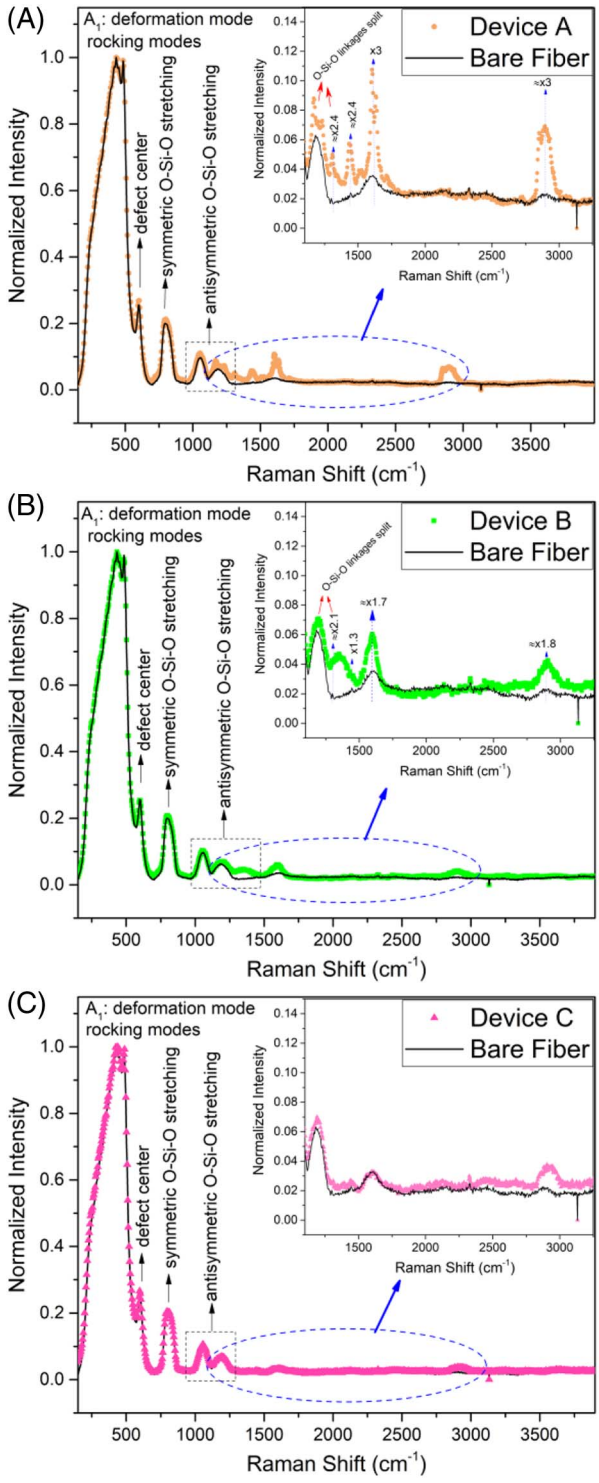

Fig. 6. Raman spectra of (A) Device A, (B) Device B, and (C) Device C. The spectra given in the insets were obtained by ×2 of the laser intensity utilized in the wide-range spectra.

We have observed the same characteristics when doubling the laser intensity, as seen in the insets of Fig. 6.

This consideration could also be consistent with the reaction mechanism provided in Eq. (3) and to the results given in Ref. [21] where the crystal-like structures on the frosted glass appears to be formed. In Devices A and C, these crystal-like structures start immediately to form when we insert the fiber into the BOE solution and go on from the solution and exposure to BOE vapor (Device C) or leave the fiber in the BOE solution (Device A).

Despite the fact that the stain-etching method is effective for the surface termination, the diameter of the CLS device is also important for good heat dissipation and long-term reliability. The effect of the tapering and the visual homogeneity of stripping were also obtained using the NIR imaging, as shown in Fig. 7. We have observed in the SEM measurements (Fig. 3) that Device A, only fabricated by the stain-etching method, was tapered excessively. As observed in Fig. 7(a), most of the unwanted cladding light was stripped at the very beginning of Device A. This is because the tapering starts at that region, so the most of the light stripped from a very small length of the fiber surface resulted in the temperature of that part rising sharply and can lead to changes in the physical properties of fiber such as RI, Young's modulus, and Poisson's ratio [22].

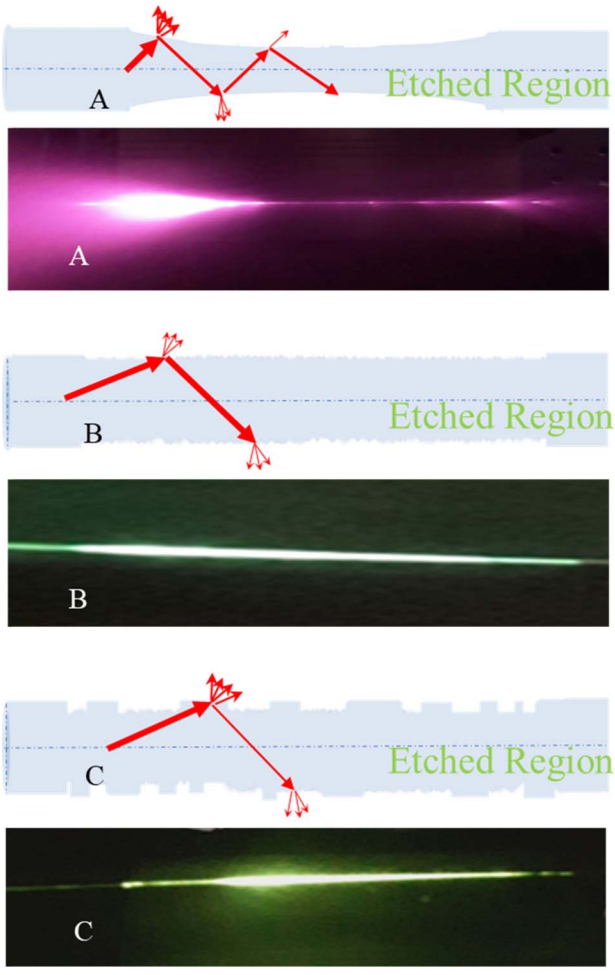

Fig. 7. Respective schematic representations of light removal mechanisms in Devices A, B, and C, and the corresponding NIR images are demonstrated.

This can finally result in fiber fuse [22,23] and damage the whole laser system. On the other hand, the diameters of Devices B and C were found to be barely changed upon the etching processes. Therefore, the tapering (~10 μm) in these devices can be ignored, since the tapering effect was not observed in the NIR image of Devices B and C, which were fabricated by the vapor-phase etching method and the combined method, respectively. As seen in Figs. 7(b) and 7(c), Devices B and C stripped the residual light in a more homogeneous manner from a longer fiber surface compared to that in Device A.

In order to understand and support the NIR images, the high-power stripping performance of the devices (A, B, C) was studied. The CLS output power was collected (Fig. 8),

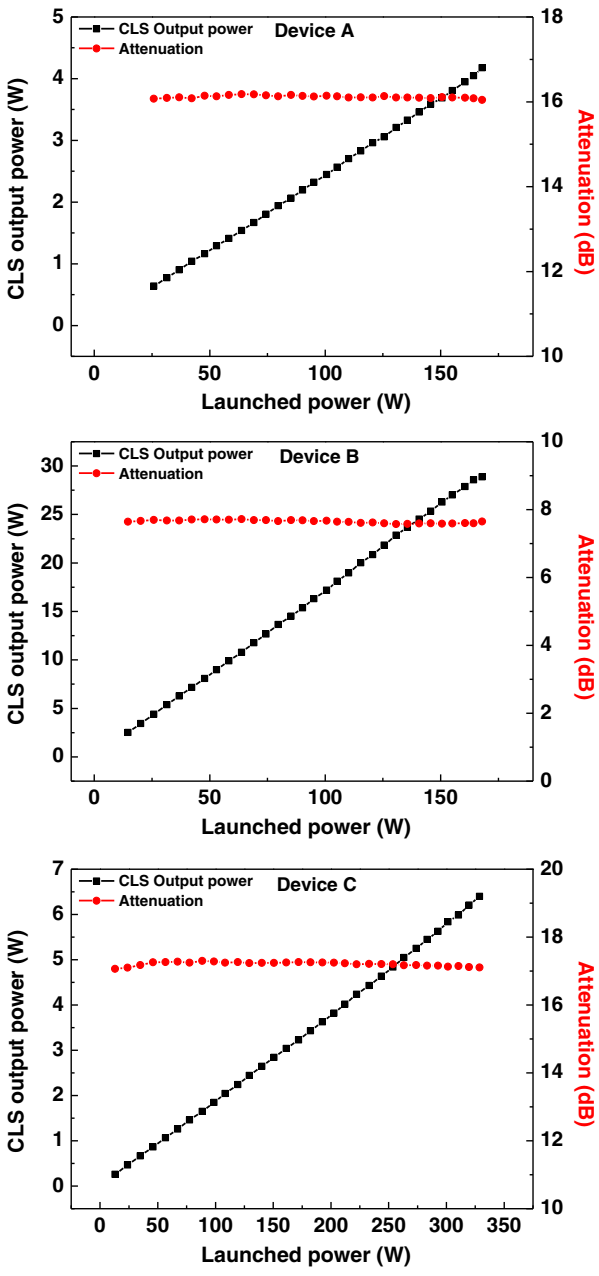

Fig. 8. Attenuation and the residual power after Device C with respect to the pump power.

and the thermal changes along the devices were observed during the performance tests. Local cladding light stripping was observed in Device A at the beginning of the CLS device as shown in the NIR image in Fig. 7(a). Thus, Device A was tested until the launched power of 170 W. The stripping performance of this device was almost constant and recorded to be 16 dB, as shown in Fig. 8, and thermal behavior of the device was 56.6°C at 100 W launched power.

Despite the uniform distribution of the stripped light, Device B was found to be incapable of removing unwanted light sufficiently; thus, the performance test was conducted by a maximum of 170 W launched power. The temperature of Device B was measured to be 57°C at 140 W launched power; however, the stripping performance was below 8 dB (Fig. 8, Device B).

Furthermore, the performance test of Device C obtained using the combined method was carried out until the launched power of 333 W (pump limited). The stripping performance of Device C was found to be ∼17.2 dB (Fig. 8) and 75.7° at the maximum launched power [Fig. 8(a)]. The stripping performance of Device C can be considered to be close to that of Device A; however, Device C manages to work at much higher launch powers. The reason for Device C removing such high-power cladding light is due to having mainly two different scattering structures, including the crystal-like shapes and the nanosized hillocks. The distribution of such high temperature load on different structures could also let the device work safely for longer durations. Furthermore, we also report the CLS performance of these three devices for multiple samples in Data File 1, Ref. [24] as shown in the Supplementary Materials. The results demonstrate that the combined method yields a mean cladding light stripping efficiency of 15.3 dB ± 1.6 dB, which can be considered to be quite sufficient for the use of removal of the most (> %97) of the cladding light.

We then investigated the long-term stripping behavior of Device C at maximum launched power of 333 W [Fig. 9(a)]. There is no change in the temperature of Device C at the end of 20 min [Fig. 9(b)]. This indicates that Device C is capable of working at long-term operation, as may be required in high-power laser applications. This can also mean that the larger diameter and the special structures of Device C designed to handle the high-power cladding light serve to have a larger surface area, yielding improvement in the distribution of heat caused by stripping the excess clad light along the device. Therefore, the safe operation of the cladding light stripping at relatively much higher launched powers was managed for Device C.

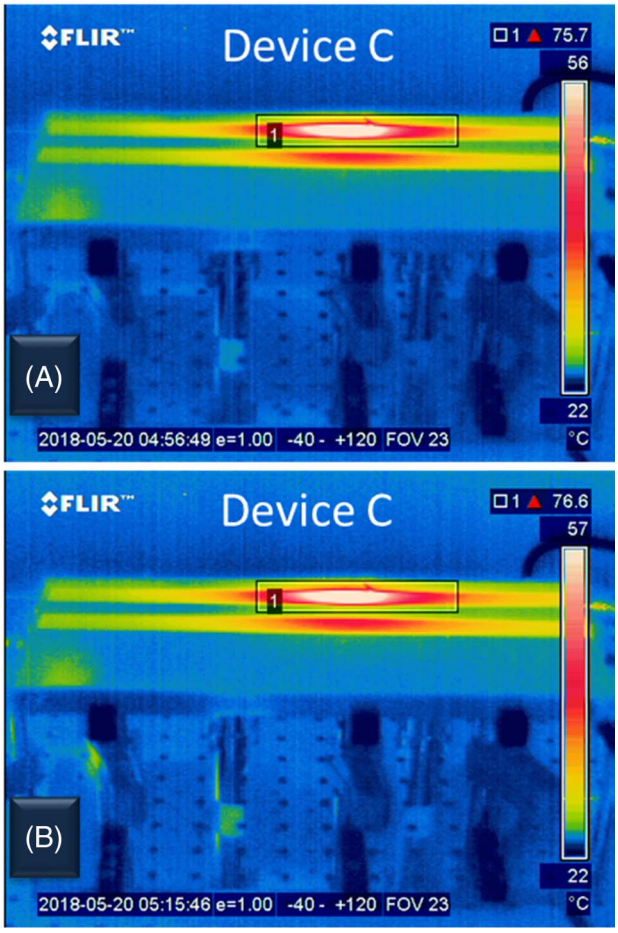

Fig. 9. Thermal images of (A) Device C and (B) Device C after 20 min CLS performance.

4. CONCLUSION

In summary, a high-power CLS at ∼17.2 dB (∼98% of the incident light and pump limited) was demonstrated with no local heat along the device using a combined method of the stain etching and vapor-phase etching. The results reveal that only stain etching gives a device that was found be extremely tapered and quite gentle to handle. On the other hand, the performance of the CLS device obtained using only the vapor-phase etching was ∼7 dB (∼80% of the incident light), giving a residual unstripped pump light, which could be unsafe at the launched power on the order of kilowatts. We observed in the SEM that the combined method gives both the crystal-like structures and nanosized hillocks observed from the stain etching and vapor-phase etching methods, respectively. Furthermore, the crystal-like structures on the surface of Devices A and C are the same in morphology; however, the AFM images show that the heights in Device C were relatively much higher than that in Device A. The latter is a key criterion for high-power CLS performance.

Funding. Türkiye Bilimsel ve Teknolojik Araştirma Kurumu (113A055).

Acknowledgment. We thank S. Yaşar and L. Ersoy for technical support.

REFERENCES

1. A. Kliner, K.-C. Hou, M. Plötner, C. Hupel, T. Stelzner, T. Schreiber, R. Eberhardt, and A. Tünnermann, "Fabrication and evaluation of a 500 W cladding-light stripper," in *Advanced Solid-State Lasers Congress* (OSA, 2013), Vol. **8616**, paper AM2A.3.
2. L. Yin, M. Yan, Z. Han, H. Wang, H. Shen, and R. Zhu, "High power cladding light stripper using segmented corrosion method: theoretical and experimental studies," Opt. Express **25**, 8760–8776 (2017).

3. P. Yan, J. Sun, Y. Huang, D. Li, X. Wang, Q. Xiao, and M. Gong, "Kilowatt-level cladding light stripper for high-power fiber laser," Appl. Opt. **56**, 1935–1939 (2017).
4. W. Guo, Z. Chen, H. Zhou, J. Li, and J. Hou, "Cascaded cladding light extracting strippers for high power fiber lasers and amplifiers," IEEE Photon. J. **6**, 1–6 (2014).
5. K. Boyd, N. Simakov, A. Hemming, J. Daniel, R. Swain, E. Mies, S. Rees, W. A. Clarkson, and J. Haub, "CO_2 laser-fabricated cladding light strippers for high-power fiber lasers and amplifiers," Appl. Opt. **55**, 2915–2920 (2016).
6. S. Boehme, K. Hirte, S. Fabian, C. Hupel, T. Schreiber, R. Eberhardt, and A. Tünnermann, "CO_2 laser-based coating process for high power fiber application," Proc. SPIE **8968**, 89680Z (2014).
7. T. Li, J. Wu, Y. Sun, Y. Wang, and Y. Ma, "An improved method for stripping cladding light in high power fiber lasers," Proc. SPIE **9255**, 92550M (2015).
8. L. Bansal, V. R. Supradeepa, T. Kremp, S. Sullivan, and C. Headley, "High power cladding mode stripper," Proc. SPIE **9344**, 93440F (2015).
9. R. Poozesh, A. Norouzy, A. H. Golshan, A. Roohforouz, A. Babazadeh, R. R. Nasirabad, N. T. Jafari, A. Heidariazar, K. Hejaz, A. Alavian, and A. Amidian, "A novel method for stripping cladding lights in high power fiber lasers and amplifiers," J. Lightwave Technol. **30**, 3199–3202 (2012).
10. A. Babazadeh, R. R. Nasirabad, A. Norouzey, K. Hejaz, R. Poozesh, A. Heidariazar, A. H. Golshan, A. Roohforouz, S. N. T. Jafari, and M. Lafouti, "Robust cladding light stripper for high-power fiber lasers using soft metals," Appl. Opt. **53**, 2611–2615 (2014).
11. P. Barboux, A. Laghzizil, Y. Bessoles, H. Deroulhac, and G. Trouvé, "Paradoxical crystalline morphology of frosted glass," J. Non-Cryst. Solids **345–346**, 137–141 (2004).
12. P. A. M. van der Heide, M. J. B. Hofman, and H. J. Ronde, "Etching of thin SiO_2 layers using wet HF gas," J. Vac. Sci. Technol. A **7**, 1719–1723 (1989).
13. T. Hoshino and Y. Nishioka, "Etching process of SiO_2 by HF molecules," J. Chem. Phys. **111**, 2109–2114 (1999).
14. L. Wong, T. Suratwala, M. D. Feit, P. E. Miller, and R. Steele, "The effect of HF/NH_4F etching on the morphology of surface fractures on fused silica," J. Non-Cryst. Solids **355**, 797–810 (2009).
15. G. A. C. M. Spierings, "Wet chemical etching of silicate glasses in hydrofluoric acid based solutions," J. Mater. Sci. **28**, 6261–6273 (1993).
16. C. D. Spencer and L. Ott, "The frosting of glass by mixtures containing hydrofluoric acid and alkali fluorides," J. Am. Ceram. Soc. **10**, 402–410 (1927).
17. G. E. Walrafen and J. Stone, "Raman spectral characterization of pure and doped fused silica optical fibers," Appl. Spectrosc. **29**, 337–344 (1975).
18. J. B. Bates, R. W. Hendricks, and L. B. Shaffer, "Neutron irradiation effects and structure of noncrystalline SiO_2," J. Chem. Phys. **61**, 4163–4176 (1974).
19. N. Chiodini, A. Lauria, R. Lorenzi, S. Brovelli, F. Meinardi, and A. Paleari, "Sol-gel strategy for self-induced fluorination and dehydration of silica with extended vacuum ultraviolet transmittance and radiation hardness," Chem. Mater. **24**, 677–681 (2012).
20. H. F. Shurvell, R. J. C. Brown, P. M. Fredericks, and L. Rintoul, "Low-temperature Raman spectra of polycrystalline NH_4F and ND_4F," J. Raman Spectrosc. **32**, 219–226 (2001).
21. H. Poulet and J. P. Mathieu, "Raman spectroscopic studies of the various phases of crystalline ammonium fluosilicate $(NH_4)_2SiF_6$," J. Raman Spectrosc. **5**, 193–198 (1976).
22. D. C. Brown and H. J. Hoffman, "Thermal, stress, and thermo-optic effects in high average power double-clad silica fiber lasers," IEEE J. Quantum Electron. **37**, 207–217 (2001).
23. A. Carter, B. N. Samson, K. Tankala, D. P. Machewirth, V. Khitrov, U. H. Manyam, F. Gonthier, and F. Seguin, "Damage mechanisms in components for fiber lasers and amplifiers," Proc. SPIE **5647**, 561–571 (2005).
24. E. Yapar Yildirim, A. Karatutlu, E. Teslime Balk, Y. Midilli, and B. Ortaç, "The performance tests of the devices A-C for multiple samples," figshare (2019), https://doi.org/10.6084/m9.figshare.9159677.